Since January 2020 Elsevier has created a COVID-19 resource centre with free information in English and Mandarin on the novel coronavirus COVID-19. The COVID-19 resource centre is hosted on Elsevier Connect, the company's public news and information website.

Clinical Radiology 76 (2021) 391.e33–391.e41

Contents lists available at ScienceDirect

Clinical Radiology

journal homepage: www.clinicalradiologyonline.net

Evaluation of pulmonary ventilation in COVID-19 patients using oxygen-enhanced three-dimensional ultrashort echo time MRI: a preliminary study

F. Zhao [a,b,1], L. Zheng [c,1], F. Shan [a], Y. Dai [c], J. Shen [a], S. Yang [a], Y. Shi [a], K. Xue [c], Z. Zhang [a,d,*]

[a] *Department of Radiology, Shanghai Public Health Clinical Center, Fudan University, Shanghai 201508, China*
[b] *Department of Radiology, The First Affiliated Hospital of Xiamen University, Xiamen, China*
[c] *MR Collaboration, Central Research Institute, United Imaging Healthcare, Shanghai 201800, China*
[d] *Department of the Principal's Office, Fudan University, Shanghai 200433, China*

ARTICLE INFORMATION

Article history:
Received 19 September 2020
Accepted 17 February 2021

AIM: To evaluate the lung function of coronavirus disease 2019 (COVID-19) patients using oxygen-enhanced (OE) ultrashort echo time (UTE) MRI.

MATERIALS AND METHODS: Forty-nine patients with COVID-19 were included in the study. The OE-MRI was based on a respiratory-gated three-dimensional (3D) radial UTE sequence. For each patient, the percent signal enhancement (PSE) map was calculated using the expression PSE $= (S_{100\%} - S_{21\%})/S_{21\%}$, where $S_{21\%}$ and $S_{100\%}$ are signals acquired during room air and 100% oxygen inhalation, respectively. Agreement of lesion detectability between UTE-MRI and computed tomography (CT) was performed using the kappa test. The Mann–Whitney *U*-test was used to evaluate the difference in the mean PSE between mild-type COVID-19 and common-type COVID-19. Spearman's test was used to assess the relationship between lesion mean PSE and lesion size. Furthermore, the Mann–Whitney *U*-test was used to evaluate the difference in region of interest (ROI) mean PSE between normal pulmonary parenchyma and lesions. The Kruskal–Wallis test was applied to test the difference in the mean PSE between different lesion types.

RESULTS: CT and UTE-MRI reached good agreement in lesion detectability. Ventilation measures in mild-type patients ($5.3 \pm 5.5\%$) were significantly different from those in common-type patients ($3 \pm 3.9\%$). Besides, there was no significant correlation between lesion mean PSE and lesion size. The mean PSE of COVID-19 lesions ($3.2 \pm 4.9\%$) was significantly lower than that of the pulmonary parenchyma ($5.4 \pm 3.9\%$). No significant difference was found among different lesion types.

CONCLUSION: OE-UTE-MRI could serve as a promising method for the assessment of lung function or treatment management of COVID-19 patients.

* Guarantor and correspondent: Z. Zhang, Department of Radiology, Shanghai Public Health Clinical Center, Fudan University, Shanghai 201508, China. Tel.: +86 021 37990333; fax: +86 021 57248782.
E-mail address: zhangzy_fd@126.com (Z. Zhang).
[1] The first two authors contributed equally to this work.

https://doi.org/10.1016/j.crad.2021.02.008
0009-9260/

Introduction

As of 09 June 2020, coronavirus disease 2019 (COVID-19) has been confirmed in 7,039,918 people worldwide, invading over 160 countries, and carrying a mortality of approximately 6.9%.[1] Despite public health responses aimed at controlling the disease and delaying its spread, several countries have been confronted with a critical care crisis, and more countries will almost certainly follow.[2] To date, prior research has suggested that computed tomography (CT) has a high sensitivity in the diagnosis of COVID-19, 98%, compared to real-time polymerase chain reaction (RT-PCR), with a sensitivity of 71%[3]; however, the prediction of the clinical course and prognosis of COVID-19 remains a challenge. There is an urgent need to identify patients at higher risk of developing acute respiratory failure so that they can be monitored closely and receive intervention treatment early.

The clinical course of COVID-19 often meets the Berlin definition of acute respiratory distress syndrome (ARDS); however, as a specific disease, the distinctive features of COVID-19 are severe hypoxaemia often associated with near-normal respiratory system compliance, which has seldom been seen in previous severe ARDS.[4] These severely hypoxaemic patients, despite sharing a single aetiology—severe acute respiratory syndrome coronavirus 2 (SARS-CoV-2)—may present with different phenotypes, and the degrees of ventilatory responsiveness may be quite different from one another.[5] In addition, accumulating evidence suggests that patients with COVID-19 have the potential for defective lung function and might suffer long-term impacts from the disease. For instance, a prospective longitudinal study of 90 patients with COVID-19-associated pneumonia found that 94% of discharged patients still had evidence of disease on their final CT.[6] This evidence included the persistence of ground-glass opacities (GGOs), which, in some patients, increased as they recovered enough to be discharged.[6] GGOs are hazy white opaque structures found on CT images, which are commonly seen in pneumonia and lung cancer. Therefore, it remains to be determined whether current COVID-19 patients will experience long-term dysfunction, similar to how some SARS patients experienced long-term lung function abnormalities.[7]

Once severe lung damage occurs, efforts should be made to suppress inflammation and manage the symptoms. As such, there is a need for a quantitative pulmonary function test that might be helpful in treatment decision-making and prognosis management. Functional magnetic resonance imaging (MRI) techniques, such as hyperpolarised helium 3 (^{3}He) MRI and, more recently, the less expensive alternative oxygen enhanced (OE) MRI, have been used to assess regional ventilation abnormalities of the lung. Three-dimensional radial ultrashort echo time (3D-UTE) MRI has shown promise as an OE-MRI method. This method does not require specialised multinuclear hardware or expensive specialty gas while providing full chest images of regional ventilation. With this technique, Kruger *et al.* performed whole-lung OE imaging in humans[8] and reported a comparison of ventilation defect distribution and signal intensity between OE-UTE-MRI and hyperpolarised ^{3}He MRI.[9] Zha *et al.* further suggested that 3D-UTE MRI supports quantitative differentiation between diseased and healthy lungs with excellent test–retest repeatability.[10]

The goal of this study was to investigate the pulmonary ventilation of patients with COVID-19 with different severities, including both pulmonary parenchyma and lesions, using OE-UTE-MRI.

Materials and methods

Patients

This study was approved by the institutional review board, and written informed consent from all patients was obtained. In this single-institution prospective study, patients diagnosed with COVID-19 according to the results of RT-PCR were recruited during the period from 25 March 2020 to 27 April 2020. Patients were divided into four groups based on the guidelines of the National Health Commission (7th edn; in Chinese)[11]: (1) mild type: mild clinical symptoms without pneumonia on imaging; (2) common type: fever, respiratory symptoms, and pneumonia manifestations on imaging. Common CT manifestations included GGOs, consolidation, and reticular and crazy-paving pattern.[12] Among these lesions, GGO is defined as hazy increased lung attenuation with preservation of bronchial and vascular margins. Consolidation is defined as opacification with obscuration of margins of vessels and airway walls.[13] The crazy-paving pattern is characterised by scattered or diffuse ground-glass attenuation with superimposed interlobular septal thickening and intralobular lines[14]; (3) severe type: respiratory distress, respiratory rate $\geq$30 times/min; resting-state oxygen saturation $\leq$93%; $PaO_2/FiO_2 \leq$300 mmHg; (4) critical type: respiratory failure requiring mechanical ventilation, shock, and other organ failure requiring intensive care unit (ICU) monitoring and treatment. Only mild-type and common-type COVID-19 patients were included in this study because most severe- and critical-type COVID-19 patients cannot endure MRI examinations, and some of them were transferred to the ICU immediately. In addition, all the patients included in this study only received basic supportive treatment without any special intervention during the CT and MRI examinations. Pulmonary function tests had not been performed in order to minimise the risk of exposure to COVID-19 infection. The exclusion criteria were as follows: (a) interval between CT and OE-UTE-MRI longer than 1 day; (b) poor MRI image quality; and (c) inability to undergo the OE-UTE-MRI examination.

Image acquisition

All patients underwent both chest CT and MRI examinations, including OE-UTE-MRI, with an interval of no more than 1 day between scans. The chest CT was performed with

a 64-section scanner (Scenaria 64 CT; Hitachi Medical, Kashiwa, Chiba Prefecture, Japan) with the patient scanned in a supine position during end-inspiration without intravenous contrast medium. Before CT imaging, all the patients received the training for breath-hold CT (including "breath in", "breath out" and "hold your breath"). They were instructed by the breathing commands during the CT examinations. The imaging parameters were as follows: 120 kV tube voltage, 150–400 mA tube current 1.5 pitch, 1 mm slice thickness, 1 mm reconstructive thickness, 350 mm collection diameter, 350 mm reconstruction diameter, 350 ms rotation time, 512 × 512 matrix, and three acquisitions.

MRI was performed using a 3 T MRI machine (uMR 780, United Imaging Healthcare, Shanghai, China) with a commercial phased-array 12-channel torso coil. Patients were in a supine position during the whole examination. The protocols included (a) transverse T2-weighted fast spin echo sequence (FSE; repetition time [TR]=3,965 ms, echo time [TE]=90.3 ms, flip angle [FA]=120°, section thickness=5 mm, field of view (FOV)=380 × 380 mm^2, matrix=456 × 456); (b) coronal T2-weighted single shot fast spin echo sequence (SS-FSE; TR=1,000 ms, TE=85.3 ms, FA=120°, slice thickness=5 mm, FOV=380 × 380 mm^2, matrix=325 × 408); and (c) a respiratory-gated 3D-UTE pulse sequence (TR=2.2 ms, TE=0.08 ms, slice thickness=2 mm, FOV=350 × 350 mm^2, matrix=480 × 480). For optimisation purposes, the FA for the 3D-UTE pulse sequence was set to 8° to maximise the absolute signal difference and contrast after OE-UTE-MRI.[8] All the patients were instructed to breathe evenly during the UTE-MRI examination and the acquisition time varied from 4–5minutes depending on the respiration status of the individual patients.

The OE-UTE-MRI of the lungs was performed with a 3D-UTE sequence as in a previous study.[15] For this technique, the entire thoracic cavity was excited with a nonselective hard pulse, followed by the acquisition of a free induction decay (FID) signal instead of an echo (as in the case of most conventional clinical sequences), resulting in a centre-out radial encoding trajectory. Signal acquisition was initiated during the ramp-up stage of the encoding gradient to further reduce the effective echo time as well as potential susceptibility artefacts as a result of air–tissue boundaries in the lungs. The direction of the encoding gradient was incremented from one acquisition to another to cover the whole k-space in a "Koosh ball" pattern.[16] A total of 40,000 encoding directions were prescribed. To alleviate the effects of respiratory motion, the UTE sequence was interleaved with a navigator sequence to track the diaphragm displacement in the superior–inferior direction. The acquisition module was enabled only within a certain predetermined displacement range, during which 2,000 FIDs were collected each time. During reconstruction, the radial k-space data were first re-gridded onto Cartesian coordinates using a Kaiser–Bessel convolution kernel.[17] A 3D fast Fourier transform was subsequently performed to generate the final image.

For OE-UTE-MRI measurement, oxygen was delivered through a nonrebreather mask placed over the subject's nose and mouth. 3D-UTE was performed twice for each subject. The first was acquired during free-breathing with 21% oxygen (normoxic), while the second was acquired with 100% oxygen (hyperoxic). Two minutes of 100% oxygen inhalation was performed before the second UTE measurement to avoid the transit effect. The duration of whole MRI acquisition was about 20 minutes.

Image analysis

To assess the feasibility of UTE-MRI in the diagnosis of COVID-19, all the CT and normoxic UTE-MRI images were randomised and analysed independently by two radiologists (one with more than 6 years of experience in chest CT diagnosis and 3 years of experience in pulmonary MRI, and the other with more than 36 years of experience in chest CT diagnosis and 16 years of experience in pulmonary MRI). All images were anonymised and evaluated in a random order blinded to clinical data. The UTE-MRI and CT images for a single patient were read separately. The number of lesions in each image modality for each patient was recorded. Then, another two experienced radiologists (one with 8 years of experience in clinical chest CT interpretation and 4 years of experience in pulmonary MRI, and the other with 19 years of experience in clinical chest CT interpretation and 8 years of experience in pulmonary MRI) evaluated independently the lesion detectability of UTE-MRI with CT as the reference. For each lesion, a five-point visual scoring system (1, absent; 2, probably absent; 3, equivocal; 4, probably present; 5, present) was applied.

Percent signal enhancement (PSE) was used to quantify pulmonary ventilation in this study. To avoid the negative impact from noise from the high-resolution normoxic and hyperoxic images on the quality of the PSE maps, the images were reconstructed at 1 cm resolution to improve the signal-to-noise (SNR).[8] After that, the high-resolution normoxic and hyperoxic images were co-registered by rigid transform and B-spline symmetric normalisation (SyN) transform[18] with a mutual information metric using Advanced Normalisation Tools (http://stnava.github.io/ANTs). The high-resolution hyperoxic images were segmented automatically to produce a binary lung mask using ITK-SNAP (www.itksnap.org).[19] After applying the deformation field from the registration and lung mask to the low-resolution data, the PSE map was computed as

$$\mathrm{PSE} = (S_{100\%} - S_{21\%})/S_{21\%} \quad (1)$$

where $S_{100\%}$ and $S_{21\%}$ represent the signal intensity of the hyperoxic and normoxic UTE images, respectively.

Lesion-based analysis was performed in consensus by two experienced radiologists. Spherical regions of interest (ROIs) with diameters of 10 mm were placed over the pulmonary parenchyma (left upper lobe, left mid-zone, left lower lobe, right upper lobe, right middle lobe and right lower lobe for each patient) on the high-resolution transverse hyperoxic images. In addition, for each COVID-19-associated lesion, the high-resolution transverse hyperoxic slice with the largest lesion area was selected as the representative slice. Lesion size was measured on the representative slice. The ROIs were then transferred to the

PSE map. The mean PSE of the pulmonary parenchyma was calculated as the average mean PSE of the six spherical ROIs, and the mean PSE for each lesion was measured.

Statistical analysis

Agreement of lesion detectability was performed using the kappa test. κ was interpreted as follows: 0.00–0.20, poor agreement; 0.21–0.40, fair agreement; 0.41–0.60, moderate agreement; 0.61–0.80, good agreement; and >0.81, very good agreement. For patient-based analysis, the Mann–Whitney *U*-test was used to evaluate the difference in the mean PSE among mild-type COVID-19 and common-type COVID-19. In common-type patients, a lesion-based analysis was carried out in which Spearman's test was used to assess the relationship between lesion mean PSE and lesion size. Furthermore, the Mann–Whitney *U*-test was used to evaluate the difference in the ROI mean PSE among normal pulmonary parenchyma and the lesions. The Kruskal–Wallis test was applied to test the difference in the mean PSE between different lesion types. Bonferroni correction was applied to reduce problems associated with multiple comparisons.

A p-value of <0.05 was considered to indicate a significant result. All statistical analyses were performed using SPSS (version 21.0, SPSS, Chicago, IL, USA).

Results

A cohort of 49 patients (age, 31.58 ± 14.43 years; range, 16–74 years) was finally included in this study. Four patients were excluded because of severe motion artefacts, two of whom coughed during the examination. Another two patients were excluded because they were unable to undergo the OE-UTE-MRI examination. A total of 35 patients (71.4%) underwent CT before MRI, while 14 patients (28.6%) underwent MRI before CT examinations.

For all the patients included in this study, the lesions detected by both CT and UTE-MRI had four typical signs (pure GGOs, GGOs with consolidation, consolidation, and crazy-paving pattern). Table 1 summarises the demographic and clinical features of the patients.

For chest CT, 159 lesions were detected in 33 patients, while for UTE-MRI, 158 lesions from 33 patients were detected. No lesions were detected in the other 16 patients. As shown in Table 2, CT and UTE-MRI reached good agreement in lesion detectability.

PSE analysis was frequently able to reveal the difference between patients with and without COVID-19-associated lesions (Fig 1). As shown in Fig 2, the mean PSE between mild-type and common-type patients was significantly different ($p=0.002$). The mean PSE of mild-type COVID-19 was 5.3 ± 5.5% (mean ± SD), while the mean PSE of common-type COVID-19 was 3 ± 3.9% (mean ± SD).

In this study, 142 out of 158 (89.9%) lesions could be readily visualised by PSE analysis (Fig 3). There was no significant correlation between lesion mean PSE and lesion size ($p>0.05$). The mean PSE of the pulmonary parenchyma ranged from 0.4% to 13.8% (mean ± SD, 5.4 ± 3.9%), while the mean PSE of the lesions was significantly lower ($p<0.001$) with a range of 0–9.4% and a mean of 3.2 ± 4.9% (Fig 4). Furthermore, no significant difference was found among different lesion types (Fig 5).

Table 1
Summary of the demographic and clinical features of the patients.

Variables	Total (n=49)
Age, years (mean ± SD)	31.58 ± 14.43
Sex male, *n* (%)	30 (61.2%)
Severities, *n* (%)	
Mild	16 (32.7%)
Common	33 (67.3%)
Symptoms, *n* (%)	
Cough	18 (36.7%)
Fever	23 (46.9%)
Chest pressure	5 (3.4%)
Sore throat	5 (3.4%)
Diarrhoea	7 (4.7%)
Lesion size, mm^2 (mean ± SD)	451.60 ± 749.53
Lesion types, *n* (%)	
Pure GGOs	25 (15.7%)
GGOs with consolidation	120 (75.5%)
Consolidation	11 (6.9%)
Crazy-paving pattern	3 (1.9%)
Imaging-positive, *n* (%)	33 (67.3%)

SD, standard deviation; GGOs, ground glass opacities; RT-PCR, real-time polymerase chain reaction.

Discussion

Currently, high-resolution chest CT is the routine and preferred method for providing morphological information on COVID-19 pneumonia. The CT findings of COVID-19 pneumonia have been reported widely; however, there is an unmet need to develop non-invasive and effective biomarkers of COVID-19 to monitor pulmonary ventilation and evaluate lung function in affected patients. A recent preprint study carried out a pulmonary function test in 137 patients with COVID-19 pneumonia 2 weeks after discharge and suggested that the pulmonary function of patients with COVID-19 pneumonia manifested as restrictive ventilation

Table 2
Result of lesion detectability between CT and UTE-MRI.

Radiological findings	Method	Visual score					κ[a]	*p*-Value
		1	2	3	4	5		
Pure GGOs	CT	134	0	0	3	22	0.678	<0.05
	UTE	135	0	3	10	11		
GGOs with consolidation	CT	39	0	1	5	114	0.444	<0.05
	UTE	39	2	7	53	58		
Consolidation	CT	148	0	0	0	11	0.903	<0.05
	UTE	148	0	0	2	9		
Crazy-paving pattern	CT	156	0	0	0	3	1	<0.05
	UTE	156	0	0	0	3		
All lesions	CT	477	0	1	8	150	0.709	<0.05
	UTE	478	2	10	65	81		

CT, computed tomography; UTE, ultrashort echo time; MRI, magnetic resonance imaging; GGOs, ground glass opacities.

[a] κ was interpreted as follows: 0.00–0.20 indicates poor agreement; 0.21–0.40, fair agreement; 0.41–0.60, moderate agreement; 0.61–0.80, good agreement; and >0.81, very good agreement.

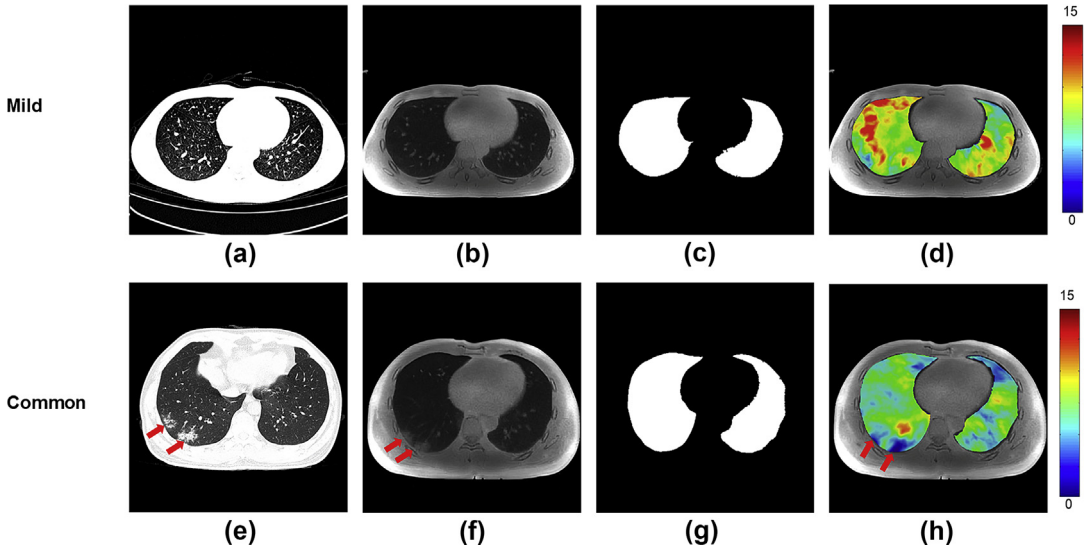

Figure 1 Patient-based analysis for mild-type and common-type COVID-19. (a) CT image from a mild-type patient without lesions. (b) Hyperoxic transverse UTE-MRI image from a mild-type patient without lesions. (c) Mask generated from (b). (d) PSE map for the mild-type patient. (e) CT image from a common-type patient with two COVID-19-related lesions. (f) Hyperoxic transverse UTE-MRI image from a common-type patient with two COVID-19-related lesions. (g) Mask generated from (f). (h) PSE map for the common-type patient.

disorder and small airway obstruction.[20] In addition, as secondary ARDS carries risk factors affecting the prognosis of COVID-19 and causes high mortality,[21] evaluating lung function and monitoring the risk of ARDS are crucial not only for diagnosis but also for prognosis.

Although CT is able to visualise lung ventilation by using dual-energy scanners, exposure to ionising radiation can be detrimental, especially when repeated examinations are required. MRI has been used to evaluate different lung diseases with the advantage of detailed soft-tissue contrast and a lack of radiation.[22] In lung imaging, conventional MRI is challenging in that the extremely short T2* of the lung parenchyma, which is due to the low hydrogen proton density in this tissue, leads to very low signal intensity obtained in the lungs. In UTE-MRI, projection acquisition of the FID in conjunction with radial readout technically makes it possible to obtain a sufficient SNR with short TE and to reduce the sensitivity to motion.[23] Previously, 3D-UTE-MRI had good concordance with CT in assessing cystic fibrosis,[24,25] quantifying lung parenchymal density,[26] and detecting pulmonary nodules.[27] The present study demonstrated that 3D-UTE-MRI was also in good agreement with CT for COVID-19 lesion detectability, which is in accordance with prior research.[28] More importantly, the complementarity of structure and function afforded by OE-MRI with UTE can provide a framework for interpreting the functional severity of structural abnormalities in lung diseases. This study further indicated the potential of OE-UTE-MRI in measuring pulmonary ventilation and performing early diagnosis.

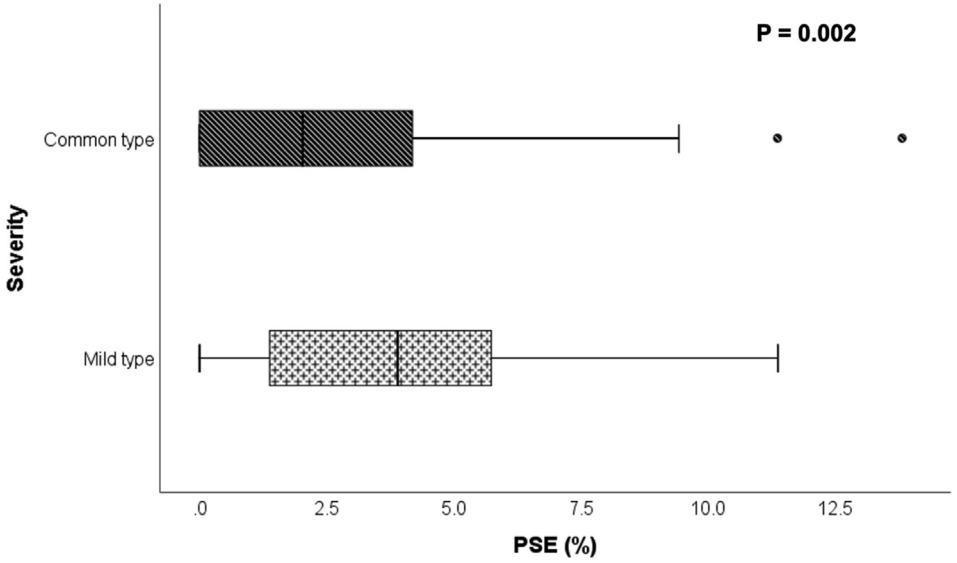

Figure 2 Comparison of the PSE between mild-type patients and common-type patients using the Mann–Whitney *U*-test.

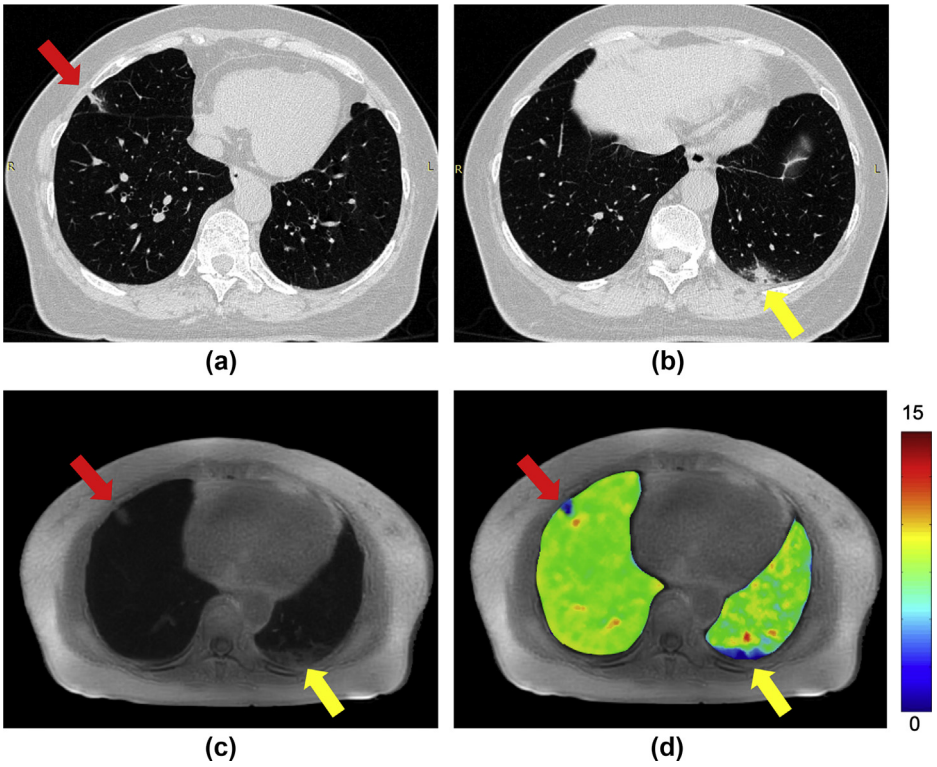

Figure 3 Representative lesion-based analysis of a 62-year-old female patient. (a) Lesion 1 (red arrow) on a CT image with radiological findings of GGO with consolidation and visual score = 5. (b) Lesion 2 (yellow arrow) on the CT image with radiological finding: GGO with consolidation, visual score = 5. (c) Lesion 1 and lesion 2 on the transverse UTE-MRI image. Radiological findings for lesion 1 are GGO with consolidation, visual score = 3. Radiological findings for lesion 2 are GGO with consolidation, visual score = 4. (d) Manifestation of lesions 1 and 2 on the PSE map.

Another advantage of 3D-UTE-MRI is its large coverage of the whole lung in one measurement. Compared to 2D OE-MRI, this 3D technique is conducive to quantitative analysis of ventilation for the whole lung or even per lobe rather than based on ROIs. Conventional 2D OE-MRI examined small-volume measurements or ROIs that often covered only a modest portion of the lungs. It is therefore unclear whether the T1 values or mean signal enhancement observed are representative of the entire pulmonary parenchyma. Calculating the mean PSE using full lung volumes supports more accurate volumetric measurements of ventilation. Based on 3D-UTE OE-MRI, the patient-based analysis revealed that the mean PSE between mild-type (mean PSE = 5.3 ± 5.5%) and common-type (mean PSE = 3.2 ± 5%) patients was significantly different. This result suggested that subtle changes in lung function may

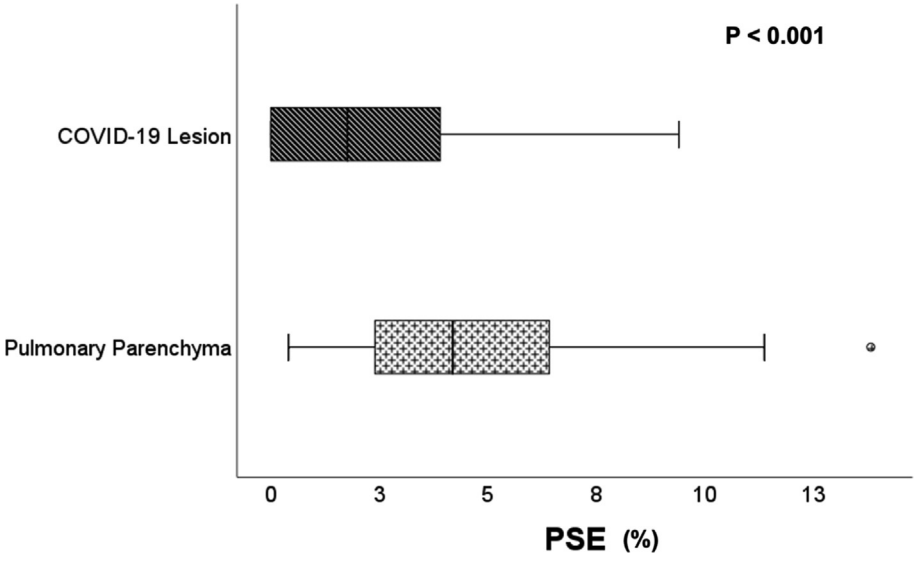

Figure 4 Comparison of the PSE between COVID-19-related lesions and pulmonary parenchyma using the Mann–Whitney *U*-test.

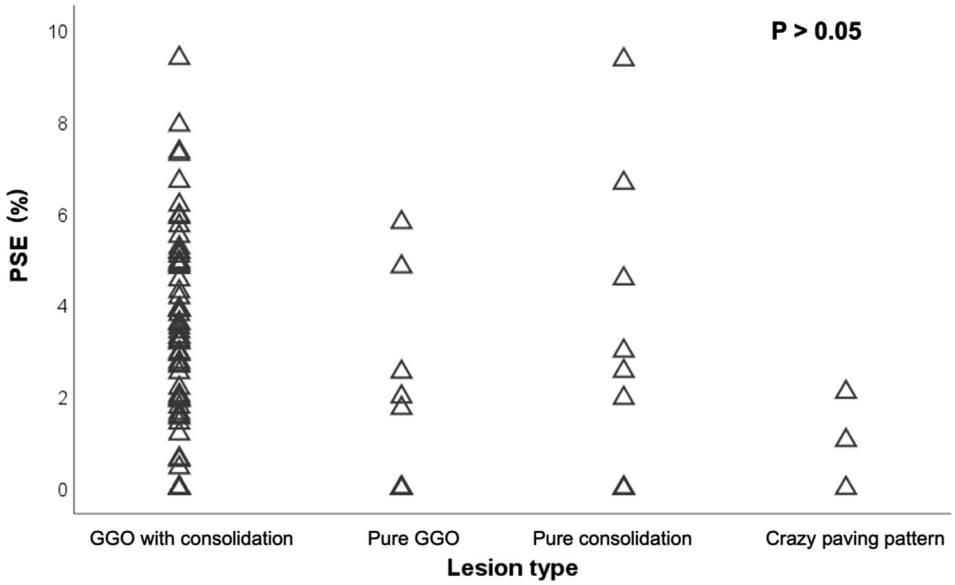

Figure 5 Comparison of PSE between different lesion types using the Kruskal–Wallis test.

reflect reduced efficiency of gas exchange and that common-type patients have worse pulmonary ventilation than mild-type patients. Previously, CT imaging had shown potential in evaluating the severity and extent of the disease[29,30]; however, two recent studies showed that clinical presentation and chest CT manifestations were sometimes unmatched. Zhang *et al.* found a patient who was clinically diagnosed as severe, but was at an early stage according to chest CT.[31] In contrast, the patients in another study showed symptom relief but progression on chest CT, indicating that clinical symptoms and imaging findings are unmatched in the early stage of COVID-19.[32] As such, OE-UTE-MRI could be a supplementary method for making diagnoses and treatment decisions. Furthermore, according to previous research, in discharged survivors with COVID-19, impairment of diffusion capacity and restrictive ventilator defects are the most common abnormalities of lung function, which are both associated with the severity of the disease.[33] OE-UTE-MRI does not involve exposure to ionising radiation and does not require expensive contrast agents or hyperpolarised gases. It could therefore be considered for application not only in diagnosis but also in routine clinical follow-up for certain recovered survivors, especially in common and severe patients.

In the present lesion-based study, there was no significant correlation between the lesion mean PSE and lesion size, probably because only common-type patients were included in this part of the study. Compared with that of the normal pulmonary parenchyma, the mean PSE of the lesions was significantly reduced ($p<0.001$). According to prior OE-MRI study, regional decreases in ventilation are common in pulmonary diseases, including lung cancer,[34] chronic obstructive pulmonary disease,[35] and asthma.[36] The measurements of regional ventilation defects from PSE maps depicts local to areas of structural abnormality. Four types of lesions were investigated in this study: GGOs, consolidations, GGOs with consolidation, and crazy-paving patterns. Consolidation is a homogeneous increase in pulmonary parenchymal attenuation that obscures the margins of vessels and airway walls.[37] Various substances may fill the air space, including fluid, blood, pus, and cells, which probably cause a regional decrease in ventilation. A previous study suggested that consolidation was associated with impairment of gas exchange and lung stiffness.[38] GGOs are caused by a partial filling of air spaces, a thickening of alveolar walls, and/or partial collapse of the alveoli.[39] Previous research also stated that an increased extent of GGOs may be correlated with a decrease in forced vital capacity.[40] According to a previous study, crazy-paving pattern lesion is related to progressive dyspnoea.[41] Thus, considering the structure and histology of COVID-19-related lesions, the result of lower mean PSE in all the lesions could be explained.

There was no significant difference between different lesion types in this study, likely attributable to a lack of consolidation ($n=11$) and the crazy-paving pattern ($n=3$). As shown in previous studies, more consolidation is found in patients with COVID-19 as the disease course progresses, and more consolidation lesions have been found in elderly patients (>50 years) than in younger patients.[42] Similarly, a crazy-paving pattern might be seen during the intermediate phase of infection (4–14 days from symptom onset).[43] As a substantial number of patients in the present study were at an early stage, this might be a possible explanation for why there were fewer complete consolidation and crazy-paving pattern lesions. This insufficiency warrants further investigation.

There were several limitations in this study. First, a small sample size, especially reflected in the lack of different lesion types, and the single-site design may affect the generalisability of the present results. Further investigations on different lesion types in a multicentre trial with a large sample size are warranted. Second, the hospital served as a quarantine hospital in this period, and no

normal control group was included in this study due to contamination of the MRI machines. Therefore, it is difficult to determine the extent to which pulmonary ventilation changes in COVID-19 patients versus normal controls. Third, the disparity between CT and UTE-MRI lung volumes during imaging acquisition and the time interval between imaging will probably affect the comparative results between CT and UTE-MRI. Fourth, considering the safety and effectiveness of the imaging examinations, COVID-19 patients at severe and critical stages were not included in this study, reducing the comprehensiveness of its results. Fifth, all the ROIs were drawn manually, which might limit the reproducibility of the measured values. An automated technique for lobar ventilation measurements from OE-MRI is needed in future research. This would enable more accurate assessment of the impact of regional ventilation by the lesions detected.

In summary, the regional and whole-lung oxygen enhancement observed on UTE-MRI in the present study suggested that OE-UTE-MRI could serve as a promising method in the evaluation of lung function in patients with COVID-19. OE-UTE-MRI is feasible to stratify the severity of COVID-19 according to mean PSE, which may help guide the treatment, evaluate treatment response, predict prognosis and identify patients who require earlier intervention.

Conflict of interest

The authors declare the following financial interests/personal relationships which may be considered as potential competing interests: Three authors (Liyun Zheng, Yongming Dai and Ke Xue) are affiliated with United Imaging Healthcare.

Acknowledgements

The authors thank Qi Liu, Jian Zhang and Xia Zhao from United Imaging Healthcare for UTE sequence developing. The authors also thank Shuheng Zhang from United Imaging Healthcare for UTE protocol adjustment. This study received funding from the Novel Coronavirus Special Research Foundation of the Shanghai Municipal Science and Technology Commission (no. 20441900600 to Zhiyong Zhang). Three authors (L.Z., Y.D., and K.X.) are affiliated with United Imaging Healthcare.

References

1. Coronavirus disease. (COVID-2019) situation report — 141. https://www.who.int/docs/default-source/coronaviruse/situation-reports/20200609-covid-19-sitrep-141.pdf?sfvrsn=72fa1b16_2. (Accessed June 10, 2020).
2. Arabi YM, Murthy S, Webb S. COVID-19: a novel coronavirus and a novel challenge for critical care. *Intens Care Med* 2020;**46**(5):833–6.
3. Fang Y, Zhang H, Xie J, *et al*. Sensitivity of chest CT for COVID-19: comparison to RT-PCR. *Radiology* 2020;**296**(2):E115–7.
4. Gattinoni L, Coppola S, Cressoni M, *et al*. Covid-19 does not lead to a "typical" acute respiratory distress syndrome. *Am J Resp Crit Care Med* 2020;**201**(10):1299–300.
5. Gattinoni L, Chiumello D, Caironi P, *et al*. COVID-19 pneumonia: different respiratory treatments for different phenotypes? *Intens Care Med* 2020;**46**:1099–102.
6. Wang D, Hu B, Hu C, *et al*. Clinical characteristics of 138 hospitalized patients with 2019 novel coronavirus–infected pneumonia in Wuhan, China. *JAMA* 2020;**323**(11):1061–9.
7. Ng C, Chan J, Kwan T, *et al*. Six month radiological and physiological outcomes in severe acute respiratory syndrome (SARS) survivors. *Thorax* 2004;**59**(10):889–91.
8. Kruger SJ, Fain SB, Johnson KM, *et al*. Oxygen-enhanced 3D radial ultrashort echo time magnetic resonance imaging in the healthy human lung. *NMR Biomed* 2014;**27**(12):1535–41.
9. Kruger SJ, Nagle SK, Cadman RV, *et al*. Comparison of regional ventilation defect distribution between oxygen-enhanced and hyperpolarized He-3 MRI. In: Proceedings of the 22nd Annual Meeting of ISMRM, Milan, Italy; 2014. Abstract 0770.
10. Zha W, Kruger SJ, Johnson KM, *et al*. Pulmonary ventilation imaging in asthma and cystic fibrosis using oxygen-enhanced 3D radial ultrashort echo time MRI. *J Magn Reson Imaging* 2018;**47**(5):1287–97.
11. General Office of National Health Committee. Notice on the issuance of a program for the diagnosis and treatment of novel coronavirus (2019-nCoV) infected pneumonia (trial revised seventh edition). Available at: http://www.nhc.gov.cn/yzygj/s7653p/202003/46c9294a7dfe4cef80dc7f5912eb1989.shtml. [Accessed 20 March 2020].
12. Wang L, Wang C, Lin B, *et al*. Imaging manifestations of COVID-19. In: Zhang M, Lin B, editors. *Diagnostic imaging of Novel coronavirus pneumonia*. Singapore: Springer Singapore; 2020. p. 23–38.
13. Hansell DM, Bankier AA, MacMahon H, *et al*. Fleischner Society: glossary of terms for thoracic imaging. *Radiology* 2008;**246**(3):697–722.
14. Rossi SE, Erasmus JJ, Volpacchio M, *et al*. "Crazy-paving" pattern at thin-section CT of the lungs: radiologic-pathologic overview. *RadioGraphics* 2003;**23**(6):1509–19.
15. Robson MD, Gatehouse PD, Bydder M, *et al*. Magnetic resonance: an introduction to ultrashort TE (UTE) imaging. *J Comput Assist Tomogr* 2003;**27**(6):825–46.
16. Mendes Pereira L, Wech T, Weng A, *et al*. UTE-SENCEFUL: first results for 3D high-resolution lung ventilation imaging. *Magn Reson Med* 2019;**81**(4):2464–73.
17. Beatty PJ, Nishimura DG, Pauly JM. Rapid gridding reconstruction with a minimal oversampling ratio. *IEEE Trans Med Imaging* 2005;**24**(6):799–808.
18. Tustison NJ. Explicit B-spline regularization in diffeomorphic image registration. *Front Neuroinformatics* 2013;**7**:39.
19. Yushkevich PA, Piven J, Hazlett HC, *et al*. User-guided 3D active contour segmentation of anatomical structures: significantly improved efficiency and reliability. *Neuroimage* 2006;**31**(3):1116–28.
20. Lv D, Chen X, Mao L, *et al*. Pulmonary function of patients with 2019 novel coronavirus induced pneumonia: a retrospective cohort study. *Ann Palliat Med* 2020;**9**:3447–52.
21. Wu C, Chen X, Cai Y, *et al*. Risk factors associated with acute respiratory distress syndrome and death in patients with coronavirus disease 2019 pneumonia in Wuhan, China. *JAMA Intern Med* 2020;**180**(7):934–43.
22. Biederer J, Hintze C, Fabel M. MRI of pulmonary nodules: technique and diagnostic value. *Cancer Imaging* 2008;**8**(1):125.
23. Ohno Y, Takahashi M, Koyama H, *et al*. Challenges of using 3 T MR systems and whole-body MRI for lung imaging. In: *MRI of the lung*. Cham, Switzerland: Springer; 2016. p. 479–505.
24. Dournes G, Menut F, Macey J, *et al*. Lung morphology assessment of cystic fibrosis using MRI with ultra-short echo time at submillimeter spatial resolution. *Eur Radiol* 2016;**26**(11):3811–20.
25. Martini K, Gygax C, Benden C, *et al*. Volumetric dynamic oxygen-enhanced MRI (OE-MRI): comparison with CT Brody score and lung function in cystic fibrosis patients. *Eur Radiol* 2018;**28**(10):4037–47.
26. Higano NS, Fleck RJ, Spielberg DR, *et al*. Quantification of neonatal lung parenchymal density via ultrashort echo time MRI with comparison to CT. *J Magn Reson Imaging* 2017;**46**(4):992–1000.
27. Cha MJ, Park HJ, Paek MY, *et al*. Free-breathing ultrashort echo time lung magnetic resonance imaging using stack-of-spirals acquisition: a feasibility study in oncology patients. *Magn Reson Imaging* 2018;**51**:137–43.

28. Yang S, Zhang Y, Shen J, *et al*. Clinical potential of UTE-MRI for assessing COVID-19: patient-and lesion-based comparative analysis. *J Magn Reson Imaging* 2020;**52**(2):397–406.
29. Zhao W, Zhong Z, Xie X, *et al*. Relation between chest CT findings and clinical conditions of coronavirus disease (COVID-19) pneumonia: a multicenter study. *AJR Am J Roentgenol* 2020;**214**(5):1072–7.
30. Li K, Fang Y, Li W, *et al*. CT image visual quantitative evaluation and clinical classification of coronavirus disease (COVID-19). *Eur Radiol* 2020;**30**(8):4407–16.
31. Zhang B, Zhang J, Chen H, *et al*. Unmatched clinical presentation and chest CT manifestation in a patient with severe coronavirus disease 2019 (COVID-19). *Quant Imaging Med Surg* 2020;**10**(4):871.
32. Hu X, Chen J, Jiang X, *et al*. CT imaging of two cases of one family cluster 2019 novel coronavirus (2019-nCoV) pneumonia: inconsistency between clinical symptoms amelioration and imaging sign progression. *Quant Imaging Med Surg* 2020;**10**(2):508.
33. Mo X, Jian W, Su Z, *et al*. Abnormal pulmonary function in COVID-19 patients at time of hospital discharge. *Eur Resp J* 2020;**55**(6):2001217.
34. Ohno Y, Hatabu H, Takenaka D, *et al*. Oxygen-enhanced MR ventilation imaging of the lung: preliminary clinical experience in 25 subjects. *AJR Am J Roentgenol* 2001;**177**(1):185–94.
35. Ohno Y, Iwasawa T, Seo JB, *et al*. Oxygen-enhanced magnetic resonance imaging versus computed tomography: multicenter study for clinical stage classification of smoking-related chronic obstructive pulmonary disease. *Am J Resp Crit Care Med* 2008;**177**(10):1095–102.
36. Zhang W-J, Niven RM, Young SS, *et al*. Dynamic oxygen-enhanced magnetic resonance imaging of the lung in asthma—initial experience. *Eur J Radiol* 2015;**84**(2):318–26.
37. Austin J, Müller NL, Friedman PJ, *et al*. Glossary of terms for CT of the lungs: recommendations of the nomenclature committee of the fleischner society. *Radiology* 1996;**200**(2):327–31.
38. Lynch DA, Hirose N, Cherniack RM, *et al*. Bleomycin-induced lung disease in an animal model: correlation between computed tomography-determined abnormalities and lung function. *Acad Radiol* 1997;**4**(2):102–7.
39. Barreto MM, Rafful PP, Rodrigues RS, *et al*. Correlation between computed tomographic and magnetic resonance imaging findings of parenchymal lung diseases. *Eur J Radiol* 2013;**82**(9):e492–501.
40. Park HJ, Lee SM, Song JW, *et al*. Texture-based automated quantitative assessment of regional patterns on initial CT in patients with idiopathic pulmonary fibrosis: relationship to decline in forced vital capacity. *AJR Am J Roentgenol* 2016;**207**(5):976–83.
41. Maimon N, Paul N, Downey GP. Progressive dyspnea associated with a crazy-paving appearance on a chest computed tomography scan. *Can Resp J* 2006;**13**(5):269–71.
42. Liu M, Zeng W, Wen Y, *et al*. COVID-19 pneumonia: CT findings of 122 patients and differentiation from influenza pneumonia. *Eur Radiol* 2020;**30**(10):5463–9.
43. Chua F, Armstrong-James D, Desai SR, *et al*. The role of CT in case ascertainment and management of COVID-19 pneumonia in the UK: insights from high-incidence regions. *Lancet Resp Med* 2020;**8**(5):438–40.